UNIVERSITY OF EXETER

ORE Open Research Exeter

TITLE

Measuring and modelling the thermal performance of the Tamar Suspension Bridge using a wireless sensor network

AUTHORS

de Battista, N; Brownjohn, James; Tan, HP; et al.

JOURNAL

Structure and Infrastructure Engineering

DEPOSITED IN ORE

15 January 2016

This version available at

http://hdl.handle.net/10871/19267

COPYRIGHT AND REUSE

Open Research Exeter makes this work available in accordance with publisher policies.

A NOTE ON VERSIONS

The version presented here may differ from the published version. If citing, you are advised to consult the published version for pagination, volume/issue and date of publication

Measuring and modelling the thermal performance of the Tamar Suspension Bridge using a wireless sensor network

Nicholas de Battista

Department of Civil and Structural Engineering, The University of Sheffield, Sheffield, U.K.

Institute for Infocomm Research, Agency for Science Technology and Research, Singapore

James M. W. Brownjohn

College of Engineering, Mathematics and Physical Sciences, University of Exeter, Exeter, U.K.

Hwee Pink Tan

Institute for Infocomm Research, Agency for Science Technology and Research, Singapore

Ki-Young Koo

School of Construction Engineering, Kyungil University, Kyungsan-si, Republic of Korea

Corresponding author: Nicholas de Battista

Correspondence address: Department of Civil and Structural Engineering, Sir Frederick Mappin Building, Mappin Street, The University of Sheffield, Sheffield S1 3JD, U.K.

Correspondence email: nickydebattista@gmail.com

Measuring and modelling the thermal performance of the Tamar Suspension Bridge using a wireless sensor network

A study on the thermal performance of the Tamar Suspension Bridge deck in Plymouth, U.K., is presented in this paper. Ambient air, suspension cable, deck and truss temperatures were acquired using a wired sensor system. Deck extension data were acquired using a two-hop wireless sensor network. Empirical models relating the deck extension to various combinations of temperatures were derived and compared. The most accurate model, which used all the four temperature variables, predicted the deck extension with an accuracy of 99.4%. Time delays ranging from 10 minutes to 66 minutes were identified between the daily cycles of the air temperature and of the structural temperatures and deck extension. However, accounting for these delays in the temperature – extension models did not improve the models' prediction accuracy. The results of this study suggest that bridge design recommendations are based on overly-simplistic assumptions which could result in significant errors in the estimated deck movement, especially for temperature extremes. These findings aim to help engineers better understand the important aspect of thermal performance of steel bridges. This paper also presents a concise study on the effective use of off the shelf wireless technology to support structural health monitoring of bridges.

Keywords: Monitoring; Structural design; Suspension bridges; Temperature effects; Thermal effects.

1. Introduction

Thermal loads due to temperature changes are an important consideration in the serviceability limit state design of bridges. Diurnal and seasonal temperature changes result in thermal expansion and contraction cycles, which bridge designs need to cater for. Structural elements such as expansion joints and rocker bearings allow the bridge deck to expand and contract without inducing excessive stresses in the structure. However, the effectiveness of the bridge engineer's thermal design depends on a correct understanding of the effects that temperature changes have on the static and dynamic behaviour of the bridge. Whereas ultimate limit state design of bridges is backed by

extensive knowledge coming from decades of research in material science and structural mechanics, relatively little is known about the thermal behaviour of bridge structures. The bulk of the research effort in this field is focused on the effects on dynamic properties of bridges.

The exceptions are short- and medium-span concrete (Branco & Mendes, 1993; Churchward & Sokal, 1981; Elbadry & Ghali, 1983; Fan, Brownjohn, & Yeow, 2000; Ho & Liu, 1989; Mirambell & Aguado, 1990; Potgieter & Gamble, 1983; Riding, Poole, Schindler, Juenger, & Folliard, 2007) and composite steel-concrete bridges (Dilger, Ghali, Chan, Cheung, & Maes, 1983; Emanuel & Taylor, 1985; Fu, Ng, & Cheung, 1990; Zuk, 1965), for which thermal effects have been analysed for many years. These types of bridges come in a variety of cross-sections and generally consist of self-supporting spans. Their thermal behaviour is largely governed by the temperature profile within the deck structure, which can be predicted depending on the geometry and material composition of the cross-section, bridge location, and time-dependent climatic factors. Larsson & Karoumi (2011) developed a finite element model to predict internal temperature distributions based on climatic information, which they validated with measured temperature records from the New Svinesund Bridge (concrete arch bridge, 704 m total span) between Sweden and Norway. Long-term monitoring projects, such as the ones carried out on the Calgary LRT Bow River bridge (prestressed concrete) (Maes, Dilger, & Ballyk, 1992) and the Confederation Bridge (prestressed concrete, 45 x 250 m main spans) (Cheung et al., 1997; Li, Maes, & Dilger, 2004) in Canada, have been instrumental in improving the understanding of temperature distributions and actions on concrete bridges.

In contrast, investigations on the quasi-static thermal performance of large steel bridges are limited to a few structures, mostly in Asia. These types of bridges are

structurally complex, relying on several load-bearing elements such as steel cables and towers, all of which influence the thermal movement of the bridge deck. One of the earliest published studies on steel bridges was carried out on the Beachley Viaduct (self-supporting, 58-64 m spans) / Wye Bridge (cable-stayed, 235 m main span) in the UK (Capps, 1968), where temperature distributions and displacements across the expansion joint were measured and compared with predictions of extreme values derived from a model based on shade air temperature and solar radiation data. Nearly four decades later, data-driven linear models relating the deck displacement at the expansion joint to the deck temperature were derived for the Ting Kau Bridge (cable-stayed, 448 m and 475 m main spans) in Hong Kong (Ni, Hua, Wong, & Ko, 2007) and the Runyang Bridge (suspension, 1490 m main span) in China (Ding & Li, 2011). However, neither of these studies considered the temperature of other structural members, which were likely to have directly influenced the deck displacement.

Cao, Yim, Zhao, and Wang (2010) identified temperature distributions and time lags for various structural members of the Zhanjiang Bay Bridge (cable-stayed, 480 m main span) in China, and how these influenced the displacement of the bridge deck and towers. Since their results were based on four days of data collected during summer, the interesting findings of this study are not necessarily indicative of the general thermal behaviour of the bridge. Probably the most comprehensive study on steel bridges to date in this field involved the use of finite element heat transfer analysis and field monitoring data to investigate the temperature distribution and thermal response of the Tsing Ma Bridge (suspension, 1377 m main span) in Hong Kong (Xia, Chen, Bao, & Xu, 2010; Xia, Chen, Zhou, & Xu, 2012; Y.-L. Xu & Xia, 2012). Due to significant differences between the climates of Asian and European countries, the thermal performance results

reported from studies on bridges in Asia might not be directly applicable to European bridges.

The scarcity of detailed investigations on the thermal performance of steel bridges is primarily due to the difficulty and high cost of instrumenting these complex structures. The Tamar Suspension Bridge (Figure 1) in the U.K. provides an example of how bridge management and academic researchers can work together to improve the engineering community's knowledge. Thanks to a collaboration with the Tamar Bridge and Torpoint Ferry Joint Committee, the Tamar Bridge has been the subject of on-going research by the Vibration Engineering Section (VES) at The University of Sheffield since 2005 (Brownjohn & Carden, 2008; Brownjohn et al., 2009; Brownjohn, Pavic, Carden, & Middleton, 2007; Cross, Worden, Koo, & Brownjohn, 2010; Koo, Brownjohn, List, Cole, & Wood, 2010).

This paper presents new insight gained on the thermal behaviour of the Tamar Suspension Bridge, building on previous findings (de Battista, Westgate, Koo, & Brownjohn, 2011), which showed the dependence of the quasi-static displacement response of the bridge deck on several structural and environmental factors. The aim of the present investigation is to improve the engineering community's understanding of how temperature changes affect the performance of suspension bridges. This study differs from previous publications in that it focuses, in particular, on how the extension-contraction cycle of the bridge deck is related to the combined changes in the temperatures of the air, suspension cable, deck and supporting truss. Six months of temperature data, acquired from a permanently installed environmental and structural monitoring system, and longitudinal deck motion data, acquired using a recently installed wireless sensor network, were used. Empirical models were fitted to the deck extension and all the possible combinations of the four temperature variables. By

comparing the prediction accuracies of all the models, it is argued that the thermally-induced longitudinal movement of the bridge deck is a complex phenomenon involving the combined actions of several structural elements.

1.1. The Tamar Suspension Bridge

Completed in 1961, the Tamar Bridge is a symmetrical suspension bridge having a total length of 563 m over three spans (Figure 2). Reinforced concrete towers (the Saltash tower to the west and the Plymouth tower to the east) rise 73 m above their caisson foundations at either end of the 335 m-long main span. These towers support two steel suspension cables (350 mm diameter) and 16 steel stay cables (100 m diameter). 5.5 m-deep longitudinal and cross trusses made of welded hollow-box steel sections are suspended from steel hangers, which are attached to the suspension cables at 9.1 m intervals. The trusses support a lightweight orthotropic steel deck with an asphalt topping, which provides four vehicle lanes and one pedestrian walkway. The walkway and one of the vehicle lanes are cantilevered off the sides of the truss. The cantilevers wrap around the outside of the Plymouth tower and provide longitudinal continuity to the truss from the Plymouth abutment to the Saltash tower. Expansion joints in the deck, cantilevers and main truss at the Saltash tower allow differential longitudinal and rotational movement between the Saltash side span (114 m long) and the rest of the deck (449 m long). A detailed description of the Tamar Bridge's structure and monitoring instrumentation can be found in Koo, Brownjohn, List, and Cole (2012).

1.2. Bridge thermal design – current practice and shortcomings

In order to examine the current level of understanding of thermal effects on bridges, the Eurocode 1 (EC1) (European Committee for Standardization, 2003) European design standard is taken as an example of structural engineering codes of practice. Section 6 of

EC1 provides engineers with guidance on calculating the thermal loads which a bridge should be expected to either accommodate or sustain, based on regional records of shade air temperatures (isotherms). From these it is assumed that one can derive the maximum and minimum extreme temperatures that a bridge deck can attain throughout its lifetime, and hence the thermal movement that needs to be catered for in its design. Several other bridge design codes give recommendations based on this methodology, some of which take into consideration vertical temperature gradients over the cross-section of a bridge deck (see for example, clause 3.1.7.1 of the NMDOT code (New Mexico Department of Transportation, 2005), section 3.12 of the AASHTO code (American Association of State Highway and Transportation Officials, 2012) and section 2.4 of the Hong Kong Highways Department code (Hong Kong Highways Department, 2006)).

However, as will be shown in this paper, the thermal behaviour of a complicated structure like a suspension bridge is not necessarily dependent only on the ambient air temperature. Design codes and numerical analyses based on this overly simplistic assumption may not be able to predict the temperature distribution and thermal movement of a bridge with sufficient accuracy (Moorty & Roeder, 1992). In order to compensate for this, it is common practice for design codes to specify safety factors, either on the expected temperature ranges or on the estimated thermal movement. While the use of safety factors is widely accepted as good engineering practice, the lack of detailed knowledge about the thermal behaviour of complex bridge structures can sometimes lead to excessively over-estimated thermal movements. Even worse, despite the use of safety factors, serviceability failures such as locked expansion joints (Cao et al., 2010) or component failure (Hornby, Collins, Hill, & Cooper, 2012) can occur, leading to questions about the extreme ranges and accumulation of displacement.

Temporal weather conditions are a major source of uncertainty. For example, the temperatures of the main structural components of a bridge may be considerably different from each other, and from the air temperature, at any point in time. This is due to direct solar radiation during sunny periods, which results in differential heat gain. Consequently, elements with large, exposed surface areas, such as the bridge deck, attain significantly higher temperatures than the air temperature, or than elements which are shaded, such as the structure under the deck. EC1 acknowledges that temperature differences can exist between the various structural elements of a bridge, but it does not give any recommendations on how to deal with them.

The effect of temporal weather variation on differential heat gain on the Tamar Bridge can be seen in Figure 3. When the weather is sunny, the temperatures of the different elements vary widely, with those elements which are exposed to direct sunshine (the suspension cable and, especially, the deck which has a large, dark surface area) achieving higher temperatures than the air temperature. However, when the weather is overcast and there is very little direct solar radiation, the variation in temperature is much less. The temperature of the truss, which is constantly shaded underneath the deck, is similar to the air temperature irrespective of the weather. Similar observations were made by Xu, Chen, Ng, Wong, and Chan (2010) when analysing seven years of temperature records from the Tsing Ma Suspension Bridge in Hong Kong. They noted that the longitudinal deck displacement was well correlated with the deck temperature, which had consistently higher monthly maxima than the air temperature. In order to cater for differential heating and cooling at the design stage, Tong, Tham, and Au (2002) proposed a method for deriving location-specific, non-linear temperature profiles over the depth of steel bridge decks. Their method is based on the statistical parameters defining the extreme distributions of air temperature and

solar radiation at the location of interest, and makes use of a mathematical model for thermal analysis of steel sections (Tong, Tham, Au, & Lee, 2001). Despite these advances, how the different temperatures of a bridge's individual structural elements affect the overall deck displacement is still a major uncertainty. In this respect, the present study contributes towards a better understanding of the thermal behaviour of bridges, in the hope that a more complete knowledge will eventually lead to better design practice.

2. Measuring the temperature and deck extension on Tamar Bridge

A structural health monitoring (SHM) system currently operating on Tamar Bridge comprises several components installed over a number of years (Koo et al., 2012). The temperature and deck extension monitoring systems, from which the data used in this study were obtained, are described in more detail in this section.

2.1. Temperature monitoring system

As part of a structural upgrade process completed in 2001 (Fish & Gill, 1997), an environmental and structural monitoring system was permanently installed on Tamar Bridge by *Fugro Structural Monitoring* (List, Cole, Wood, & Brownjohn, 2006). This wired monitoring system, which is still in operation, comprises 90 data acquisition channels, sampling at 0.1 Hz, all of which are simultaneously time-stamped. Of these, 10 channels measure the temperature at various points on the bridge (Figure 4):

- one channel measures the shade air temperature;
- one channel measures the temperature of the north suspension cable;
- four channels measure the temperature of the deck (of which, the main span temperature channel was used in this study);

- four channels (of which, one was used in this study) measure the temperature of the truss structure, at the same location, close to the mid-span of the bridge;

The air temperature is measured using a temperature probe with a radiation shield while the other temperatures are measured using platinum resistance thermometers. The instrumentation was installed four decades after the bridge was constructed, so the sensors measuring the temperature of the structural elements had to be surface mounted. Consequently, the temperature data are only point measurements and cannot represent precisely the whole structure, especially in the case of the thick suspension cable. However, in this study it was assumed that, due to the high thermal conductivity of steel, the temperature measured by the surface mounted sensors was a good approximation of the average internal and span-wise temperature of the structural elements they were attached to.

2.2. Deck extension wireless monitoring system

Two pull-wire type ASM WS12 linear potentiometers (extensometers) with a measurement range of 0-500 mm were installed on the Tamar Bridge to monitor the deck extension, starting from July 2010. They were fixed across the deck expansion joint, between the end of the main span and the Saltash tower, with one sensor at the north edge and another at the south edge of the deck (marked ‘N’ and ‘S’ respectively in Figure 4). Together they tracked the longitudinal movement of the main deck and Plymouth side span, which are structurally continuous and have a combined length of 449 m, relative to the Saltash Tower. The aim of having a sensor at each edge of the deck was to identify any possible quasi-static rotation of the main span deck about the vertical axis. However, the sensor on the south edge repeatedly experienced mechanical problems throughout the deployment. Since only a single extension measurement

channel was required for this study, and since signals acquired when both sensors were operational showed negligible difference, the extension of the bridge deck was derived solely from the north extensometer readings. The acquired data represent the relative distance between the bridge deck and the Saltash tower, with respect to an arbitrary datum. Therefore an increase in the extension reading is indicative of the deck contracting, while a decrease in the extension reading indicates that the deck is expanding.

Experience from a previous deployment of these same extensometers showed that it was not possible to connect them to one of the existing wired monitoring systems as they would cause electrical interference which would corrupt the signals from the other sensors. On the other hand, running separate data cables from the expansion joint to the data acquisition system at the Plymouth abutment would have been prohibitively expensive and time-consuming. Therefore, in this latest addition to the SHM systems on Tamar Bridge, a wireless sensor network (WSN) was used to acquire the data from the extensometers. Wireless technology is relatively new in SHM applications and it is likely to be more widely used in the future. Most applications described in the literature for monitoring civil structures make use of wireless sensors which are purpose-built and are used to capture dynamic response (Feltrin, Meyer, Bischoff, & Motavalli, 2010; Jang et al., 2010; Kurata et al., 2012; Pakzad, 2010). Hence the deployment of the WSN system on the Tamar Bridge using off the shelf units, and its performance in monitoring the quasi-static response of the bridge will be described in some detail in the following sections.

2.2.1. Wireless sensor network hardware

A National Instruments (NI) WSN was used to acquire and transmit the data from the extensometers at the Saltash tower to a data sink located approximately 470 m away, at

the bridge abutment on the Plymouth side. This distance exceeded the transmission range of the NI WSN system, which operates on the 2.4GHz frequency range using the IEEE 802.15.4 (IEEE, 2011) wireless communication standard. To overcome this, a two-hop network was set up as follows:

- The extensometers at the Saltash tower were connected to an NI WSN-3202, 4-channel, 16-bit analogue input *end node* (marked 'E' in Figure 5), which was set to read, digitise and wirelessly transmit one sample from each sensor every five seconds.
- The end node communicated with a similar NI WSN-3202 which acted as an intermediary *router node* (marked 'R' in Figure 5).
- The router node relayed information between the end node and an NI WSN-9791 Ethernet *gateway node* (marked 'G' in Figure 5), located close to the abutment on the Plymouth side.
- The gateway node was connected with an Ethernet cable to a laptop which acted as the *data sink*, located in a control chamber within the Plymouth abutment.

The location of the router node was largely dictated by its power requirement. When used as a router node, the NI WSN-3202 must remain on continuously to listen for transmissions, hence it requires a constant external power supply. The best location was thus on the main span next to the Plymouth tower, with access to an existing DC power circuit. When used as an input (end) node, the NI WSN-3202 can run on four 1.5 V batteries. However, in that case, an adequate maintenance-free lifetime would only be achievable by using a low duty cycle (the time spent in an active state as a fraction of the total time). In order to maintain continuous monitoring throughout the investigation,

the end node and the extensometers were connected to the same DC power circuit mentioned previously, which was also available at the Saltash Tower.

The layout of the WSN resulted in two communication hops of approximately 330 m and 140 m, with the former still exceeding the specified communication range of the NI WSN nodes. Following a number of range tests using different types of antennas, it was decided to replace the antenna supplied by the manufacturer on the three nodes with a third-party 10 dBi high-gain, omni-directional antenna (Figure 5), thus increasing the transmission range enough to operate the network reliably. The wireless link quality was also found to improve considerably when the nodes' antennas were within line-of-sight of each other. Therefore the antenna at each node location was fixed on top of the crash barrier running along the entire length of the bridge. While this did not provide complete line-of-sight due to the upward camber of the deck, it was the next best possible solution.

2.2.2. Data acquisition and management software

The extension data acquisition and storage were managed using a virtual instrument (VI) (Figure 6) programmed in NI LabVIEW. The VI, which also served as a real-time system observation monitor, ran continuously on the data sink laptop which was accessible remotely via a broadband internet connection. The data were time-stamped and stored on the laptop in binary files, with each file spanning 24 hours. The files were automatically copied to an off-site server computer where the data were processed to remove any unrealistic outlier values. For a single data point to be classified as an outlier it had to have a significantly larger value (by a few mm) than both the preceding and succeeding points. Any such point was clearly visible on the time history plot as a sudden spike in the data. The rationale behind this was that it was highly unlikely that the bridge deck experienced such a rapid contraction and elongation cycle within two

measurement intervals (10 s), meaning that such spikes in the data were almost certainly caused by electrical or mechanical sensor noise. After replacing the identified outlier values by the mean of the data points recorded directly before and after them, the data were then stored in a database system (Koo, de Battista, & Brownjohn, 2011).

2.2.3. Wireless communication performance

Readings indicating the quality of the wireless communication links between the nodes, measured as a percentage of the optimal link quality, were obtained every five seconds from the NI WSN system (Figure 7). As expected, the link quality of the router node – gateway node hop was generally better than that of the longer end node – router node hop. The link quality of both hops rarely fell below 20%, which is acceptable as the NI WSN can still function reliably at this level. However, the wireless network communication failed on four occasions during the six month of monitoring. As a result, deck extension data are missing over periods lasting for 3.4 hours, 23.5 days, 6.3 days and 7.9 days, starting in July, September, October and November 2010 respectively.

Whenever the wireless communication link failed, the nodes were able to re-form the network automatically once the communication environment had improved enough for the link to be restored. However, the data acquisition VI would stop and had to be reset remotely over the internet. To avoid lost time before noticing the data interruption, in subsequent software upgrades, an error-alert email function was added to the VI. This alert system still cannot overcome breakdowns caused by occasional hardware failures unrelated to the WSN, as happened in July and September 2010. On these occasions, the system remained inaccessible for 34.6 days and 23.5 days respectively, until the fault was rectified.

A closer look at the time history of the link quality (Figure 8) shows that the shorter router node – gateway node hop generally remained fairly constant throughout

the day. On the other hand, the link quality of the longer end node – router node hop showed a clear diurnal, cyclic pattern. Due to the long transmission distance in this hop, the wireless communication is more susceptible to interference. The most likely culprit for the drops in link quality during the daytime is the interference caused by the increase in traffic crossing the bridge. Metallic surfaces, such as vehicles, attenuate radio signals and the effect is more noticeable the weaker the signal is. The greater number of vehicles in close proximity to the WSN's antennas during the day seems to have been detrimental to the radio communication link between the end and router nodes.

3. Modelling the temperature - extension relationship of the bridge deck

Data collected over a period of six months, from 1st July to 31st December 2010, were used in this investigation. The air, suspension cable, deck and truss temperatures (T_{air}, T_{cable}, T_{deck} and T_{truss} respectively), measured in °C, were obtained from the Structural Monitoring System. The deck extension (E), measured in mm, was acquired from the north extensometer. The extreme values recorded over this period are shown in Table 1. It is interesting to note that, while the minimum temperatures were all recorded on the same day, the maximum and largest peak to peak cable and deck temperatures occurred on different days from those of the air and truss temperatures. This shows that temperature extremes of the structural elements do not necessarily coincide with each other or with air temperature extremes. Maximum temperatures of elements exposed to direct solar radiation are largely dependent on the absence of cloud cover, as shown in Figure 3.

The aim of this study was to gain a better understanding of the relationship between the extension of the bridge deck and the various temperatures by deriving a model that could accurately represent the data. This temperature – extension relationship was initially assumed to be of a linear polynomial (LP) form:

$$\begin{aligned} E(t) &= \beta + \{\alpha_{air} T_{air}(t) + \alpha_{cable} T_{cable}(t) + \alpha_{deck} T_{deck}(t) + \alpha_{truss} T_{truss}(t)\} + \varepsilon(t) \\ &= \beta + \mathbf{AT}(t) + \varepsilon(t) \end{aligned} \quad (1)$$

where $E(t)$ is the measured distance between the bridge deck and the Saltash tower (the deck extension) at time t; β is a constant; $\mathbf{T}(t) = [T_{air}(t) \quad T_{cable}(t) \quad T_{deck}(t) \quad T_{truss}(t)]'$ are the measured temperatures of the air, suspension cable, deck and truss respectively at time t; having weighting coefficients $\mathbf{A} = [\alpha_{air} \quad \alpha_{cable} \quad \alpha_{deck} \quad \alpha_{truss}]$ respectively; and $\varepsilon(t)$ is the residual or error term which accounts for measurement noise and uncertainties arising from any factors that are not accounted for in the model. The weighting coefficients in **A** are synonymous with, and have the same units as, the coefficient of thermal expansion (mm/°C).

3.1. Theoretical background: model estimation using regression analysis

Regression analysis using a least squares approach can be used to estimate the unknown β and α parameters in the LP model shown in equation (1), leading to the approximate model:

$$\begin{aligned} \hat{E}(t) &= \hat{\beta} + \{\hat{\alpha}_{air} T_{air}(t) + \hat{\alpha}_{cable} T_{cable}(t) + \hat{\alpha}_{deck} T_{deck}(t) + \hat{\alpha}_{truss} T_{truss}(t)\} \\ &= \hat{\beta} + \hat{\mathbf{A}}\mathbf{T}(t) \end{aligned} \quad (2)$$

where ^ is added on β and α to indicate that they are estimated values, and $\hat{E}(t)$ is the extension predicted by the estimated model. Following the model parameter estimation, which is carried out on a sub-set of the measured data (the training data set), the prediction accuracy of the approximate model is then tested against the remaining data (the validation data set).

The sample by sample prediction errors are commonly expressed as the root mean squared error (RMSE), defined as:

$$RMSE = \left(\frac{1}{n_v} \sum_{i=1}^{n_v} \left(E_i - \hat{E}_i \right)^2 \right)^{1/2} \quad (3)$$

where n_v is the number of samples in the validation data set. The fit of the estimated model can then be assessed on the basis of the normalised root mean squared error (NRMSE), defined as:

$$NRMSE = \left(\frac{RMSE}{E_{\max} - E_{\min}} \right) \cdot 100\% \quad (4)$$

where E_{max} and E_{min} are the maximum and minimum values of the measured response variable in the validation data set, respectively.

3.2. Pre-processing the temperature and extension data

To provide a more manageable data set, the data collected over the six month period were summarised to 48 values per day for each variable, on every hour and half hour, resulting in 8832 data points (Figure 9). Each value was taken as the mean of the raw data collected from two minutes before to two minutes after the time at which the value occurred. This data reduction also helped to smooth the time histories and reduce measurement noise. Due to occasional failures of the data acquisition systems, some of the half-hourly values were not available. Therefore the final data sets used in this study consisted of 8794 half-hourly samples (equivalent to 183.2 days) for each of the temperature variables and 5301 half-hourly samples (equivalent to 110.4 days) for the extension variable. Out of these, all the temperature and extension data were available in 5268 half-hourly samples (equivalent to 109.8 days).

3.3. Linear polynomial model fitting and validation

In order to identify which temperature variables can be used to best predict the deck

extension, an exploratory data analysis was carried out on LP models with all possible combinations of one, two, three or four temperature variables. This was equivalent to setting three, two, one or none of the α coefficients in the approximate model in equation (2) to zero, respectively. Thus, 15 different models (one main model and 14 nested models) were estimated and their performance compared. This was done using a ten-fold cross-validation technique (Browne, 2000; Geisser, 1975) on the 5268 samples where data for all the temperature and extension variables was available, as summarised in the flowchart in Figure 10. This statistical procedure involved randomly allocating the data samples to ten sub-sets of 526 samples each (the remaining eight samples were discarded). Of these, nine sub-sets were used as the model training data (4734 samples). The remaining sub-set was used as the validation data (526 samples).

An ordinary least squares regression analysis was carried out on the training and validation data sets, for each of the 15 models in turn. Thus, the $\hat{\beta}$ and $\hat{\mathbf{A}}$ model parameters, as well as the prediction errors, were obtained for each model. The model fitting and validation was carried out a total of ten times, each time using a different sub-set as the validation data. This ensured that all the data samples were used for both training and validation, and that each sample was used exactly once as validation data.

In order to reduce the variability of the results, the entire cross-validation process was repeated ten times. Before each repetition, the ten data sub-sets were allocated randomly all over again. Thus 100 values of error and of the model parameters were obtained for each of the models. The mean values and standard deviations were calculated for each model's error and parameters and the prediction accuracy of each model was taken as 100% – mean(*NRMSE*).

3.4. Autoregressive model fitting to account for time lags

The LP model in equation (1) does not account for the effect of time lags between the temperature and extension arising from differential heat gain / loss. The significance of this omission on the accuracy of the derived LP models was investigated.

3.4.1. Estimation of time lags from the time domain

The time lags were first estimated by examining the time domain data. Averaged auto spectral densities of the data sets (Figure 11) confirmed that the temperatures and extension varied predominantly at a rate of one cycle per day. Therefore the data were filtered with a sixth order bandpass Butterworth filter with frequency cutoffs at 0.9 and 1.1 cycles per day, in order to retain only the frequency component at one cycle per day. The filtered data were then averaged over one-day periods and the times at which the extrema and zero-crossings of each variable occurred were recorded. From these times, initial estimates of the daily cycle time delays were obtained for each structural temperature and extension variable with respect to the air temperature.

3.4.2. Estimation of time lags from the frequency domain

Subsequently, transfer functions and coherence functions were computed between the air temperature (as the input variable) and the three structural temperatures and the deck extension (as the output variables) in turn. Using the relationship:

$$\Delta t(f) = -\frac{\phi(f)}{2\pi f} \tag{5}$$

a refined estimate of the time lags, Δt, was obtained for each of the output variables from their transfer function phase, $\phi(f)$, at the data's dominant frequency, f, of 1 cycle per day.

3.4.3. Accounting for time lags in the temperature – extension models

The refined time lag estimates from Section 3.4.2 were used to derive first order autoregressive models with exogenous inputs (ARX models) and no output feedback, having the general form:

$$E(t) = \beta + \left\{ \begin{array}{l} \alpha_{air} T_{air}(t - \Delta t_{air}) \\ + \alpha_{cable} T_{cable}(t - \Delta t_{cable}) \\ + \alpha_{deck} T_{deck}(t - \Delta t_{deck}) \\ + \alpha_{truss} T_{truss}(t - \Delta t_{truss}) \end{array} \right\} + \varepsilon(t) \qquad (6)$$

where $E(t)$, t, β, $T_x(t)$ and $\varepsilon(t)$ are as described for equation (1); α_x are the regression coefficients operating on their respective inputs (temperatures), each having a time delay of Δt_x. An ARX model of this form was derived for each of the temperature variable combinations used to estimate the LP models. The accuracy of the ARX and LP models was compared on the basis of their prediction RMSE in order to determine whether it was necessary to account for the time lags in the temperature – extension model.

4. Results and discussion

The results of the LP model fitting by cross-validation are shown in Figure 12. The model which took the deck extension to be linearly proportional to only the air temperature (model 1), had the worst prediction accuracy amongst all the models considered (95.8%). It also had the highest standard deviation for the prediction accuracy (0.18%)[1]. The maximum error in the extension prediction of this model was

[1] Higher prediction accuracy standard deviation implies lower prediction precision. Prediction precision is a measure of reproducibility, that is, the level of consistency in the model's accuracy from one prediction to another.

32.9 mm (RMSE = 7.1 mm). An error of this magnitude is generally within the tolerances catered for by engineering practice. Therefore, for a medium-span bridge such as the Tamar Bridge this level of accuracy is likely to be sufficient under normal weather conditions. However, this might not be the case when predicting deck movement under extreme temperatures and for longer bridges. In such cases, a more accurate model involving structural temperatures might be required to predict the expansion – contraction cycle of the bridge deck accurately enough.

The model which included all four temperature variables (model 15) had the best prediction performance (99.4% accuracy, 4.5 mm maximum error, 1.1 mm RMSE). Its accuracy also had the lowest standard deviation (0.02%), meaning that the model was able to predict the deck extension with high precision and consistency. Thus, the most accurate and precise temperature – extension LP model as derived from this study (model 15) is:

$$\hat{E}(t) = 91.25 + \{0.41T_{air}(t) - 0.26T_{cable}(t) - 2.50T_{deck}(t) - 3.02T_{truss}(t)\} \qquad (7)$$

The models which omitted one or two temperature variables, but included both the deck and truss temperatures, (models 10, 13 and 14) also performed well. Their prediction accuracies (all 99.3%) and errors (maximum / RMSE: 4.7 mm / 1.2 mm, 4.3 mm / 1.1 mm and 4.8 mm / 1.1 mm respectively) were very similar to those of the model with all four variables. The low standard deviation of these models' accuracy (0.03%, 0.02% and 0.03% respectively) was indicative of high precision. Therefore the model in equation (7) can be simplified to include only the deck and truss temperatures (model 10):

$$\hat{E}(t) = 90.93 + \{-2.60T_{deck}(t) - 2.77T_{truss}(t)\} \qquad (8)$$

with negligible loss of accuracy and precision.

4.1. Significance of time lags in the temperature – extension models

The initial time lag estimates (Figure 13) showed that the cable and truss temperature cycles and the deck extension cycle lagged the air temperature cycle. On the other hand, the deck temperature cycle anticipated the air temperature cycle. This is likely due to the faster heat gain and loss of the deck from its large, dark surface. These observations show that a change in the air temperature does not necessarily reflect itself immediately in the structural temperatures and in the thermal response of the bridge. Other environmental and structural factors may have a significant effect. The peak values of the truss temperature were very similar to those of the air temperature, since the truss is constantly shaded and therefore it does not gain heat by direct solar radiation. Conversely, the cable and deck, which are exposed, had a larger daily temperature gradient than the air temperature.

In the frequency domain (Figure 14), all the structural temperatures and the deck extension showed very good correlation (coherence close to 1) with the air temperature at a frequency of 1 cycle per day. The coherence between the variables deteriorated for higher frequencies, confirming that the cyclic variation of the variables occurs predominantly on a diurnal basis. The phase angle of the transfer functions at a frequency of 1 cycle per day indicates that the cable temperature, truss temperature and deck extension lagged the air temperature by 35 minutes, 66 minutes and 17 minutes respectively, while the deck temperature anticipated the air temperature by 10 minutes. These values are similar to the initial estimates obtained from the simplified time domain method shown in Figure 13. The time domain method values were intended as a validity check for the refined and more accurate frequency domain estimates listed above, with the latter being used to derive the ARX models.

The time lag estimates obtained from the transfer functions were converted into temperature time lags with respect to the deck extension so as to fit the general form of the ARX model in equation (6). Since the data points occurred at 30 minute intervals, the time lags were rounded to the nearest 30 minutes. The extension data set was then shifted by 90 minutes (3 sampling periods) so as to have only positive Δt values, resulting in the general ARX model (t in minutes):

$$E(t-90) = \beta + \left\{ \begin{array}{l} \alpha_{air} T_{air}(t-120) \\ + \alpha_{cable} T_{cable}(t-60) \\ + \alpha_{deck} T_{deck}(t-120) \\ + \alpha_{truss} T_{truss}(t-30) \end{array} \right\} + \varepsilon(t-90) \qquad (9)$$

The ARX models derived in this way infer that the extension at time t is dependent on single values of the various temperatures at some time $t - \Delta t$. While it is true that sudden environmental changes happening within the Δt period could also influence the deck extension, such events were considered to be rare outlier occurrences at the Tamar Bridge. Visual observation of the reduced data records that were used indicated that the 30 minute sampling interval was sufficient to capture any rapid changes in temperature and extension.

Despite the obvious presence of time lags between the temperature and extension data, the ARX models which accounted for these did not provide any significant improvement over the LP models. The differences in prediction accuracies between the LP models and their equivalent ARX models were less than 1 mm. The only exception was model 4 (using only the deck temperature) where the RMSE of the ARX model was 2.2 mm less than that of the LP model. Therefore there is no apparent benefit to be gained by accounting for the time lags in the temperature – extension model and the simple LP model shown in equation (8) is good enough.

4.2. Effectiveness of the linear polynomial model

It can be seen that, out of the four temperature variables considered in this study, the air temperature was the least influential on the extension prediction model. The temperatures of the deck and of the truss structure which supports it were the most important variables. The improvement in accuracy achieved by modelling the deck extension using the deck and truss temperatures, rather than any individual temperature variable alone, can be observed by comparing the two plots in Figure 15. When the extension is plotted against the raw temperature data, no linear trend can be identified (Figure 15a). The plot also shows a significant amount of scatter. However, when the deck extension is plotted against the combined deck and truss temperatures, weighted according to equation (8), the accuracy of this model is clear: the trend closely follows the theoretical straight line with very little scatter (Figure 15b). This observation also shows the initial linear polynomial model assumption to be valid, that is, that the deck extension can be modelled as a linear combination of weighted temperatures. However this might not always be the case for other bridges.

4.3. Comparison with design recommendations

From these results it is clear that the temperature – extension relationship of the Tamar suspension bridge is in fact more complicated than is commonly assumed in design practice (which is largely in line with model 1). It is likely that this is also the case with other complex steel bridges. While current design assumptions might be adequate under normal weather conditions (at least for short- and medium-span bridges), a more thorough understanding of thermal actions is required to deal with temperature extremes.

To help illustrate this point, the design longitudinal deck movement due to thermal actions for Tamar Bridge was calculated using temperature isotherms, following the recommendations in Eurocode 1 (Table 2). The resulting value of 522.6 mm (row iv in Table 3) is nearly three times larger than the movement range measured during the six months of monitoring (175.9 mm). When the same EC1 procedure is used but the isotherm temperatures T_{min} and T_{max} are replaced by the measured temperature extremes (row iii in Table 3), the resulting deck extension range (452.1 mm) overestimates the measured movement by more than two and a half times. While over-design is necessary to allow for abnormal temperature extremes, such a large difference is excessive and uneconomical, as the movement range recommended by the design code would require unrealistic temperatures to occur. This is certainly not unique to the Eurocode; the AASHTO design procedure results in a similar overestimation for the Tamar Bridge (row v in Table 3). In contrast, the extension range predicted by the linear model in equation (8) (176.9 mm) matches the measured value with over 99% accuracy (row ii in Table 3). Clearly a better understanding of the thermal behaviour of complex bridges is needed to enable more efficient design practice.

5. Conclusion

A detailed examination of the thermal effects on the Tamar Suspension Bridge has been presented in this paper. The data used in this study were acquired over six months. They consisted of air, suspension cable, deck and truss temperature records and longitudinal deck extension records. The temperature data were acquired from an existing wired monitoring system while the extension data were acquired from pull-wire extensometers which were installed at the deck expansion joint specifically for this study. In order to simplify the extensometer system and reduce the installation costs, a two-hop wireless sensor network (WSN) was set up using National Instruments WSN nodes. Despite the

relatively long transmission distances between the nodes (330 m and 140 m), the WSN reliability was satisfactory, with the wireless data transmission failing on only four occasions over the six months of operation. The link quality of the longer hop was observed to deteriorate as the number of vehicles crossing the bridge increased during the day.

Fifteen different linear polynomial models relating the deck extension to various weighted combinations of temperatures were estimated empirically from the data with a least squares cross-validation approach. The models were compared based on their extension prediction accuracy. The model which included only the air temperature (similar to recommendations in bridge design codes of practice) was the least accurate (95.8% accuracy). The best prediction accuracy (99.4%) was achieved by the model that included all four temperature variables. However, by including only the deck and truss temperatures, the model could be simplified while still achieving high prediction accuracy (99.3%). Despite having identified time delays between the daily cycles of the various temperatures and the deck extension, accounting for these delays by using ARX models did not result in any significant improvement in the prediction accuracy of the temperature – extension models.

From the findings of the study presented in this paper, a numbers of conclusions can be made:

- Due to differential heating from solar radiation, one cannot assume the temperatures of the bridge's structural elements to be identical to each other or to the air temperature. At times when there is no cloud cover, elements which have a large surface area exposed to direct solar radiation (such as the bridge deck), will attain daytime temperatures which are significantly higher than those of the air. Therefore, during the design stage, it is important to account for

different parts of a bridge heating up or cooling down at different rates, and to different levels, as this has a bearing on the thermal behaviour of the whole structure.

- Contrary to common assumption in bridge design practice, one cannot accurately estimate extreme values of the expansion of a suspension bridge deck based on air temperature records. Bridge thermal design based on this assumption can lead to significantly over-estimated deck movements due to the use of large safety factors.
- On the other hand, the deck extension is closely related to and can be estimated with very good accuracy and precision from the combined temperatures of the deck and truss or girder supporting it. A better understanding of the thermal effects on medium- and long-span steel bridges is required in order to be able to predict these temperatures at the design stage (as is common practice for concrete bridges). This can only be achieved through in-service monitoring of new and existing steel bridges.
- In order to study the thermal behaviour of a bridge deck, it is important to measure at least the temperatures of the deck and of the structure that directly supports it. Measuring only the air temperature will be of little use for this purpose. Temperature data from other supporting elements, such as suspension and stay cables, could also be useful. It is recommended that structural and environmental monitoring systems are planned for in the design phase and installed on bridges during construction. In general, this would be significantly easier and more cost-effective than implementing a monitoring system on an operational bridge.

- As this study has shown, wireless sensor systems are a viable solution for medium- and long-span bridges where cable installation is problematic. WSN technology is currently advanced enough to enable reliable quasi-static data acquisition, with a number of commercial products that can be used available on the market.

This study has highlighted the lack of knowledge about the complex thermal behaviour of steel bridges and the resulting deficiencies in the design recommendations given by codes of practice. While this investigation relates to a single bridge, the Tamar Bridge in Plymouth, UK, similarly complex relationships of temperature and extension are likely to exist in other steel bridges. Whereas the numerical values of time lags and the empirical models derived in this study are not directly applicable to other bridges, the qualitative information derived from the analysis is of general interest. The conclusions listed above are expected to be valid for any medium- and long-span steel bridge. In this respect, this study and its findings are a contribution towards gaining much-needed insight into the thermal behaviour of steel bridges. Further experimental studies are needed (and hereby encouraged) on existing steel bridge structures, in order to develop sufficient knowledge on this important aspect of bridge performance. Only then can the outcome of this, and other similar monitoring-based investigations, translate into better design recommendations for future structures.

Acknowledgements

The authors would like to acknowledge the assistance given by National Instruments in providing some of the WSN equipment used in this investigation and the on-site support given by Steve Rimmer, Richard Cole and David List from the Tamar Bridge and Torpoint Ferry Joint Committee. This research was supported by EPSRC grant EP/F035403/1: Novel data mining and performance diagnosis systems for structural health monitoring of suspension bridges. The first author was supported by the joint A*STAR Research Attachment Program between the

Agency for Science, Technology and Research (A*STAR) in Singapore and The University of Sheffield, U.K.

References

American Association of State Highway and Transportation Officials. (2012). *AASHTO LRFD Bridge Design Specifications* (6th ed.). Washington, DC: AASHTO.

Branco, F. A., & Mendes, P. A. (1993). Thermal actions for concrete bridge design. *Journal of Structural Engineering*, *119*(8), 2313–2331. doi:10.1061/(ASCE)0733-9445(1993)119:8(2313)

British Standards Institution. (2007). *UK National Annex to BS EN 1991-1-5:2003. Eurocode 1. Actions on structures. General actions. Thermal actions*. London, UK: BSI.

Browne, M. (2000). Cross-validation methods. *Journal of Mathematical Psychology*, *44*(1), 108–132. doi:10.1006/jmps.1999.1279

Brownjohn, J. M. W., & Carden, P. (2008). Real-time operation modal analysis of Tamar Bridge. In *Proceedings of the 26th International Modal Analysis Conference (IMAC XXVI)*. Orlando, FL, USA.

Brownjohn, J. M. W., Pavic, A., Carden, E. P., & Middleton, C. J. (2007). Modal testing of Tamar suspension bridge. In *Proceedings of the 25th International Modal Analysis Conference (IMAC XXV)*. Orlando, FL, USA.

Brownjohn, J. M. W., Worden, K., Cross, E., List, D. I., Cole, R., & Wood, T. (2009). Thermal effects on performance on Tamar Bridge. In *Proceedings of the 4th International Conference on Structural Health Monitoring of Intelligent Infrastructure (SHMII-4)* (Zurich, Sw.). Zurich, Switzerland.

Cao, Y., Yim, J., Zhao, Y., & Wang, M. L. (2010). Temperature effects on cable stayed bridge using health monitoring system: a case study. *Structural Health Monitoring*, *10*(5), 523–537. doi:10.1177/1475921710388970

Capps, M. W. (1968). *The thermal behavior of the Beachley Viaduct/Wye Bridge* (No. LR 234). Crowthorne, UK: Road Research Laboratory.

Cheung, M. S., Tadros, G. S., Brown, T., Dilger, W. H., Ghali, A., & Lau, D. T. (1997). Field monitoring and research on performance of the Confederation Bridge. *Canadian Journal of Civil Engineering*, *24*(6), 951–962. doi:10.1139/l97-081

Churchward, A., & Sokal, Y. J. (1981). Prediction of temperatures in concrete bridges. *Journal of the Structural Division*, *107*(ST11), 2163–2176.

Cross, E., Worden, K., Koo, K. Y., & Brownjohn, J. M. W. (2010). Modelling environmental effects on the dynamic characteristics of the Tamar suspension

bridge. In *Proceedings of the 26th International Modal Analysis Conference (IMAC XXVIII)*. Jacksonville, FL, USA.

De Battista, N., Westgate, R., Koo, K. Y., & Brownjohn, J. M. W. (2011). Wireless monitoring of the longitudinal displacement of the Tamar Suspension Bridge deck under changing environmental conditions. In M. Tomizuka (Ed.), *Proceedings of SPIE: Sensors and Smart Structures Technologies for Civil, Mechanical, and Aerospace Systems* (Vol. 7981, p. 79811O). San Diego, CA, USA. doi:10.1117/12.879811

Dilger, W. H., Ghali, A., Chan, M., Cheung, M. S., & Maes, M. A. (1983). Temperature stresses in composite box girder bridges. *Journal of Structural Engineering*, *109*(6), 1460–1478. doi:10.1061/(ASCE)0733-9445(1983)109:6(1460)

Ding, Y., & Li, A. (2011). Assessment of bridge expansion joints using long-term displacement measurement under changing environmental conditions. *Frontiers of Architecture and Civil Engineering in China*, *5*(3), 374–380. doi:10.1007/s11709-011-0122-x

Elbadry, M. M., & Ghali, A. (1983). Temperature variations in concrete bridges. *Journal of Structural Engineering*, *109*(10), 2355–2374. doi:10.1061/(ASCE)0733-9445(1983)109:10(2355)

Emanuel, J. H., & Taylor, C. M. (1985). Length-thermal stress relations for composite bridges. *Journal of Structural Engineering*, *111*(4), 788–804. doi:10.1061/(ASCE)0733-9445(1985)111:4(788)

European Committee for Standardization. (2003). *Eurocode 1: Actions on structures - Part 1-5: General actions - Thermal actions (EN 1991-1-5:2003)*. Brussels, Belgium: CEN.

Fan, S. C., Brownjohn, J. M. W., & Yeow, O. C. (2000). Is BS 5400 temperature distribution applicable under Singapore conditions? *IES Journal Singapore*, *40*(5), 43–49.

Feltrin, G., Meyer, J., Bischoff, R., & Motavalli, M. (2010). Long-term monitoring of cable stays with a wireless sensor network. *Structure and Infrastructure Engineering*, *6*(5), 535–548. doi:10.1080/15732470903068573

Fish, R., & Gill, J. (1997). Tamar suspension bridge - strengthening and capacity enhancement. In B. Pritchard (Ed.), *Bridge Modification 2: Stronger and safer bridges. Proceedings of the International Conference organized by the Institution of Civil Engineers*. London, U.K.

Fu, H. C., Ng, S. F., & Cheung, M. S. (1990). Thermal behavior of composite bridges. *Journal of Structural Engineering*, *116*(12), 3302–3323. doi:10.1061/(ASCE)0733-9445(1990)116:12(3302)

Geisser, S. (1975). The predictive sample reuse method with applications. *Journal of the American Statistical Association*, *70*(350), 320–328.

Ho, D., & Liu, C.-H. (1989). Extreme thermal loadings in highway bridges. *Journal of Structural Engineering*, *115*(7), 1681–1696. doi:10.1061/(ASCE)0733-9445(1989)115:7(1681)

Hong Kong Highways Department. (2006). *Structures design manual for highways and railways* (3rd ed.). Kowloon, Hong Kong: Highways Department.

Hornby, S. R., Collins, J. H., Hill, P. G., & Cooper, J. R. (2012). Humber Bridge A-frame refurbishment / replacement. In *Proceedings of the 6th International Conference on Bridge Maintenance, Safety and Management (IABMAS)* (pp. 3170–3177). Stresa, Italy: Taylor & Francis Group, London.

IEEE. (2011). *IEEE standard for local and metropolitan area networks - Part 15.4: Low-rate wireless personal area networks (LR-WPANs)*. New York, NY, USA: Institute of Electrical and Electronics Engineers, Inc.

Jang, S., Jo, H., Cho, S., Mechitov, K. A., Rice, J. A., Sim, S.-H., … Agha, G. (2010). Structural health monitoring of a cable-stayed bridge using smart sensor technology: deployment and evaluation. *Smart Structures and Systems*, *6*(5-6), 439–459.

Koo, K. Y., Brownjohn, J. M. W., List, D. I., & Cole, R. (2012). Structural health monitoring of the Tamar suspension bridge. *Structural Control and Health Monitoring*, *20*(4), 609–625. doi:10.1002/stc.1481

Koo, K. Y., Brownjohn, J. M. W., List, D. I., Cole, R., & Wood, T. (2010). Innovative structural health monitoring for Tamar Suspension Bridge by automated total positioning system. In D. Frangopol, R. Sause, & C. Kusko (Eds.), *Proceedings of the 5th International Conference on Bridge Maintenance, Safety and Management (IABMAS2010) - Bridge Maintenance, Safety, Management, Life-Cycle Performance and Cost* (pp. 544–551). Philadelphia, PA, USA.

Koo, K. Y., de Battista, N., & Brownjohn, J. M. W. (2011). SHM data management system using MySQL databse with MATLAB and Web interfaces. In *Proceedings of the 5th International Conference on Structural Health Monitoring of Intelligent Infrastructure (SHMII-5)* (Cancun, Me.). Cancun, Mexico.

Kurata, M., Kim, J., Lynch, J. P., Van Der Linden, G. W., Sedarat, H., Thometz, E., … Sheng, L.-H. (2012). Internet-enabled wireless structural monitoring systems: Development and permanent deployment at the New Carquinez Suspension Bridge. *Journal of Structural Engineering*, (published online on 12th March 2012). doi:10.1061/(ASCE)ST.1943-541X.0000609

Larsson, O., & Karoumi, R. (2011). Modelling of climatic thermal actions in hollow concrete box cross-sections. *Structural Engineering International*, *21*(1), 74–79. doi:10.2749/101686611X12910257102550

Li, D., Maes, M. A., & Dilger, W. H. (2004). Thermal design criteria for deep prestressed concrete girders based on data from Confederation Bridge. *Canadian Journal of Civil Engineering*, *31*(5), 813–825. doi:10.1139/l04-041

List, D. I., Cole, R., Wood, T., & Brownjohn, J. M. W. (2006). Monitoring performance of the Tamar Suspension Bridge. In *Proceedings of the 3rd International Conference on Bridge Maintenance, Safety and Management (IABMAS2006)*. Porto, Portugal.

Maes, M. A., Dilger, W. H., & Ballyk, P. D. (1992). Extreme values of thermal loading parameters in concrete bridges. *Canadian Journal of Civil Engineering*, *19*(6), 935–946. doi:10.1139/l92-112

Mirambell, E., & Aguado, A. (1990). Temperature and stress distributions in concrete box girder bridges. *Journal of Structural Engineering*, *116*(9), 2388–2409. doi:10.1061/(ASCE)0733-9445(1990)116:9(2388)

Moorty, S., & Roeder, C. W. (1992). Temperature-dependent bridge movements. *Journal of Structural Engineering*, *118*(4), 1090–1105. doi:10.1061/(ASCE)0733-9445(1992)118:4(1090)

New Mexico Department of Transportation. (2005). *Bridge procedures and design guide*. Santa Fe, NM, USA: NMDOT.

Ni, Y. Q., Hua, X. G., Wong, K. Y., & Ko, J. M. (2007). Assessment of bridge expansion joints using long-term displacement and temperature measurement. *Journal of Performance of Constructed Facilities*, *21*(2), 143–151. doi:10.1061/(ASCE)0887-3828(2007)21:2(143)

Pakzad, S. N. (2010). Development and deployment of large scale wireless sensor network on a long-span bridge. *Smart Structures and Systems*, *6*(5-6), 525–543.

Potgieter, I. C., & Gamble, W. L. (1983). *Response of highway bridges to nonlinear temperature distributions* (No. SRS-505). *Civil Engineering Studies*. Urbana, IL: University of Illinois at Urbana-Champaign.

Riding, K. A., Poole, J. L., Schindler, A. K., Juenger, M. C. G., & Folliard, K. J. (2007). Temperature boundary condition models for concrete bridge members. *ACI Materials Journal*, *104*(4), 379–387.

Tong, M., Tham, L. G., & Au, F. T. K. (2002). Extreme thermal loading on steel bridges in tropical region. *Journal of Bridge Engineering*, *7*(6), 357. doi:10.1061/(ASCE)1084-0702(2002)7:6(357)

Tong, M., Tham, L. G., Au, F. T. K., & Lee, P. K. K. (2001). Numerical modelling for temperature distribution in steel bridges. *Computers & Structures*, *79*(6), 583–593. doi:10.1016/S0045-7949(00)00161-9

Xia, Y., Chen, B., Bao, Y. Q., & Xu, Y. L. (2010). Thermal behaviors of Tsing Ma Suspension Bridge. In D. Frangopol, R. Sause, & C. Kusko (Eds.), *Proceedings of the 5th International Conference on Bridge Maintenance, Safety and Management (IABMAS2010) - Bridge Maintenance, Safety, Management, Life-Cycle Performance and Cost* (pp. 2655–2661). Philadelphia, PA, USA.

Xia, Y., Chen, B., Zhou, X. Q., & Xu, Y. L. (2012). Field monitoring and numerical analysis of Tsing Ma Suspension Bridge temperature behavior. *Structural Control and Health Monitoring*, *20*(4), 560–575. doi:10.1002/stc.515

Xu, Y. L., Chen, B., Ng, C. L., Wong, K. Y., & Chan, W. Y. (2010). Monitoring temperature effect on a long suspension bridge. *Structural Control and Health Monitoring*, *17*, 632–653. doi:10.1002/stc.340

Xu, Y.-L., & Xia, Y. (2012). *Structural health monitoring of long-span suspension bridges*. Oxon, UK: Spon Press.

Zuk, W. (1965). Thermal behavior of composite bridges - Insulated and uninsulated. *Highway Research Record*, (76), 231–253.

Figures & captions

Figure 1. The Tamar Suspension Bridge in the U.K., crossing the River Tamar between Plymouth to the east and Saltash to the west.

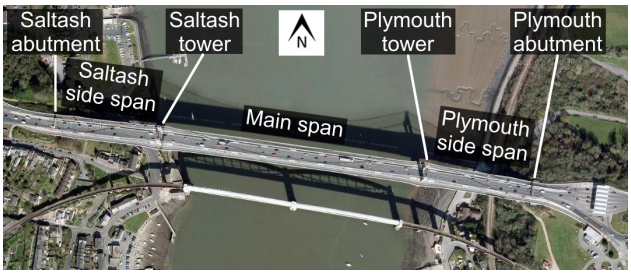

Figure 2. Aerial view of the 3-span Tamar Bridge: 114m-long side spans on either side of a 335m-long main span.

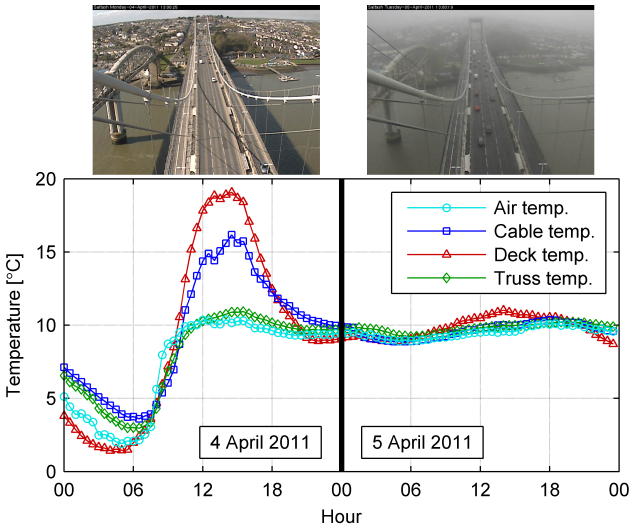

Figure 3. Temperature records on a sunny day (left plot, 4th April 2011) followed by an overcast day (right plot, 5th April 2011), showing the effect of weather-dependent differential heat gain. The photos of the Tamar Bridge (top) were both taken at 1pm on the respective days, from a west-facing webcam on the Plymouth tower.

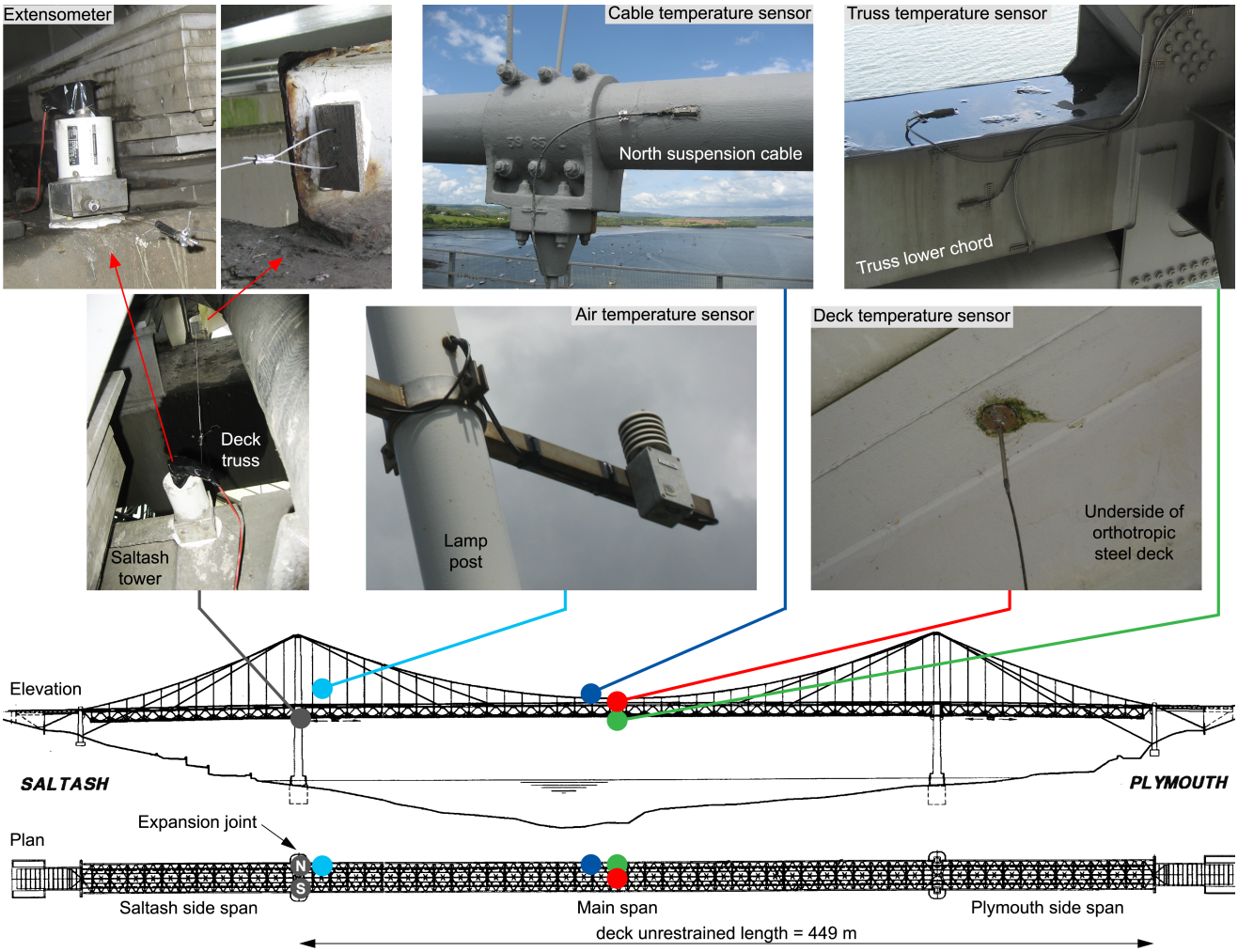

Figure 4. Location of the extensometers and temperature sensors from which the data used in this study were obtained.

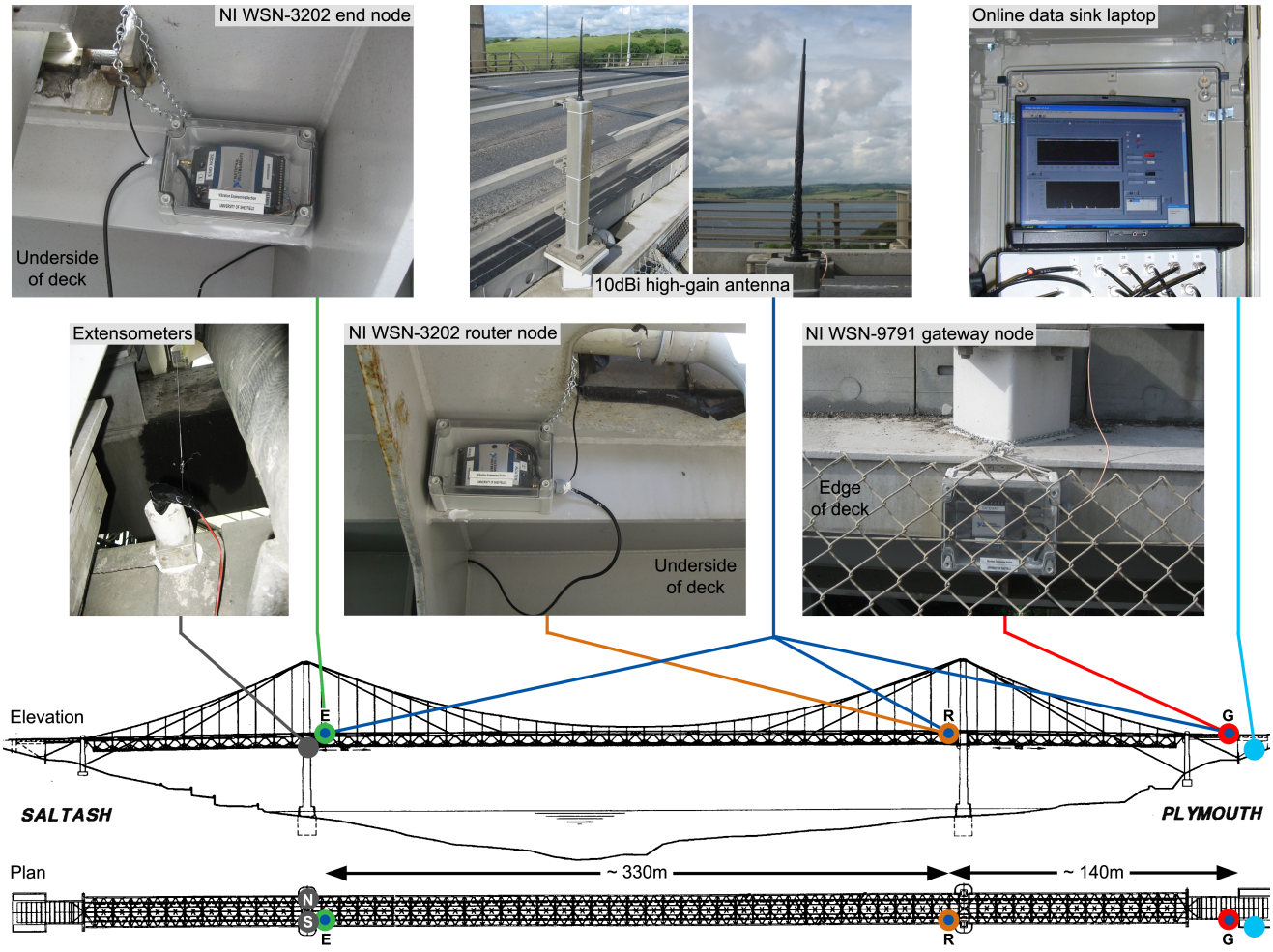

Figure 5. Location of the components making up the wireless extension monitoring system. The data acquired from the extensometers at the Saltash tower were transmitted to the data sink at the Plymouth abutment via a 2-hop wireless sensor network.

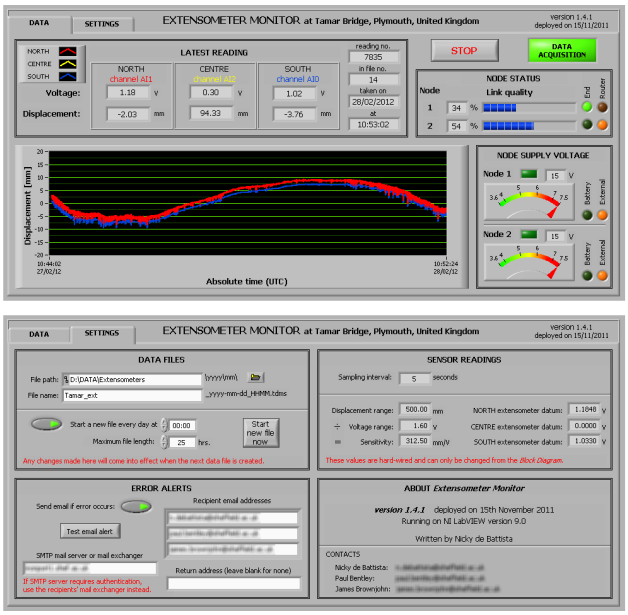

Figure 6. Screenshots of the latest version of the National Instruments (NI) LabVIEW virtual instrument (VI) used to acquire data from the extensometers. The VI provided a visualisation of the acquired extensometer data, the wireless network status, the power supply status and various settings.

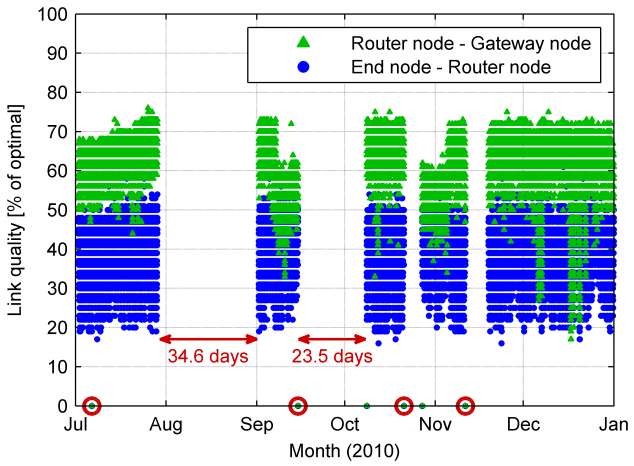

Figure 7. Time history of the wireless communication link quality over the two hops in the wireless sensor network (WSN). The red circles indicate the four occasions when the wireless link failed. The red arrows mark periods when the system was unavailable due to hardware failure unrelated to the WSN.

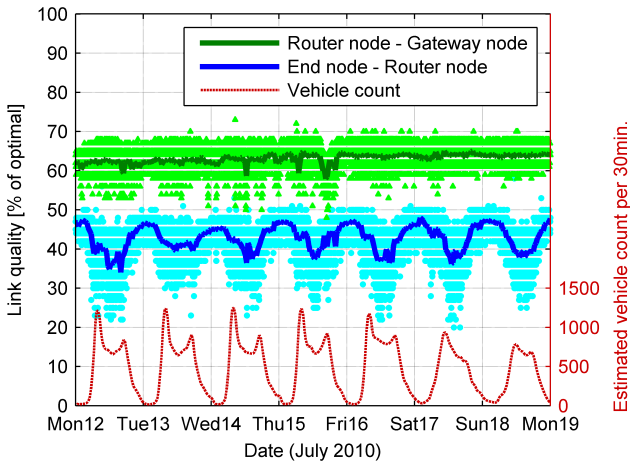

Figure 8. Comparison of the wireless communication link quality with the estimated number of vehicles crossing the bridge over one week. The thick solid lines represent half-hourly average values of the link qualities.

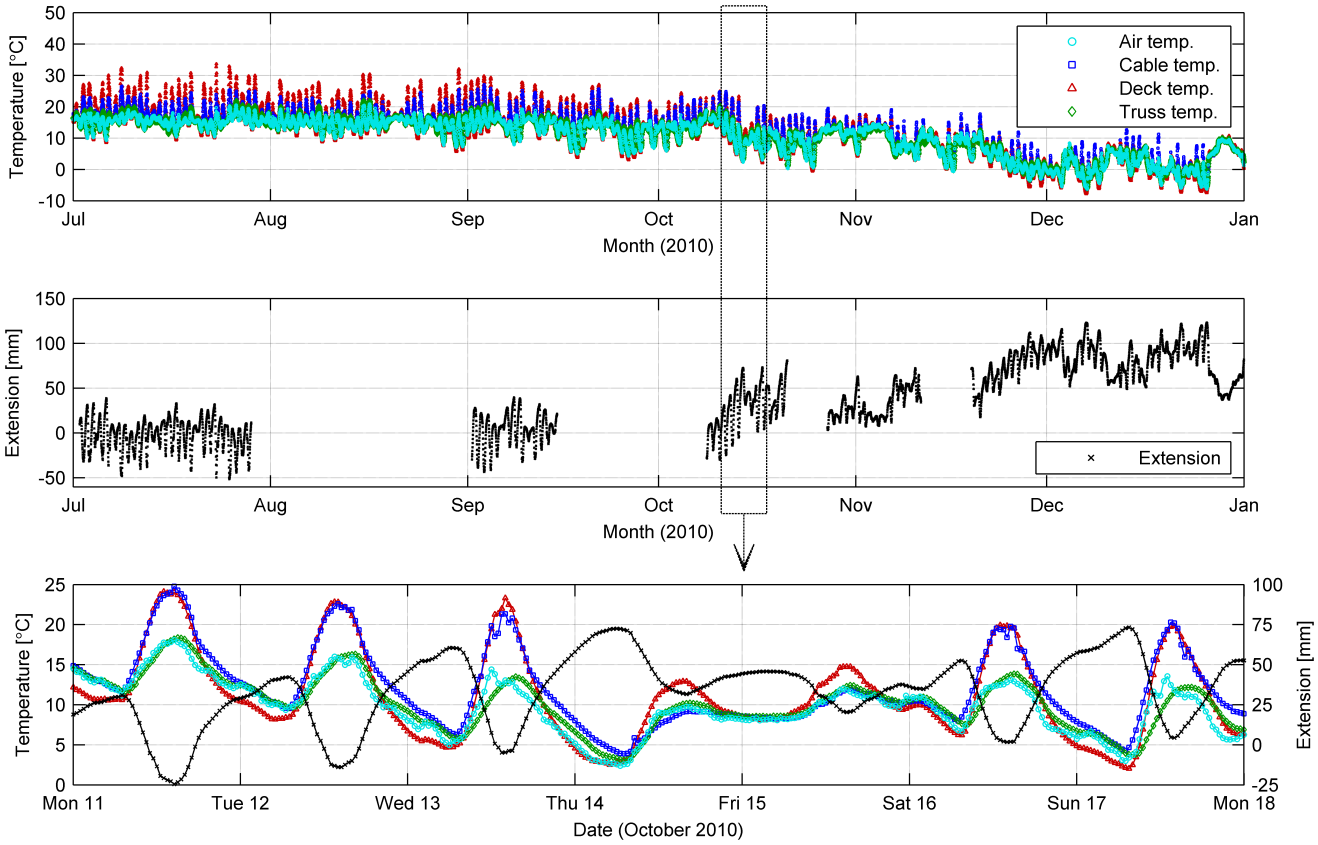

Figure 9. The resampled temperature (top) and extension (middle) data acquired over six months, and an enlarged one-week section (bottom). Note that a positive change in extension implies a contraction of the bridge deck.

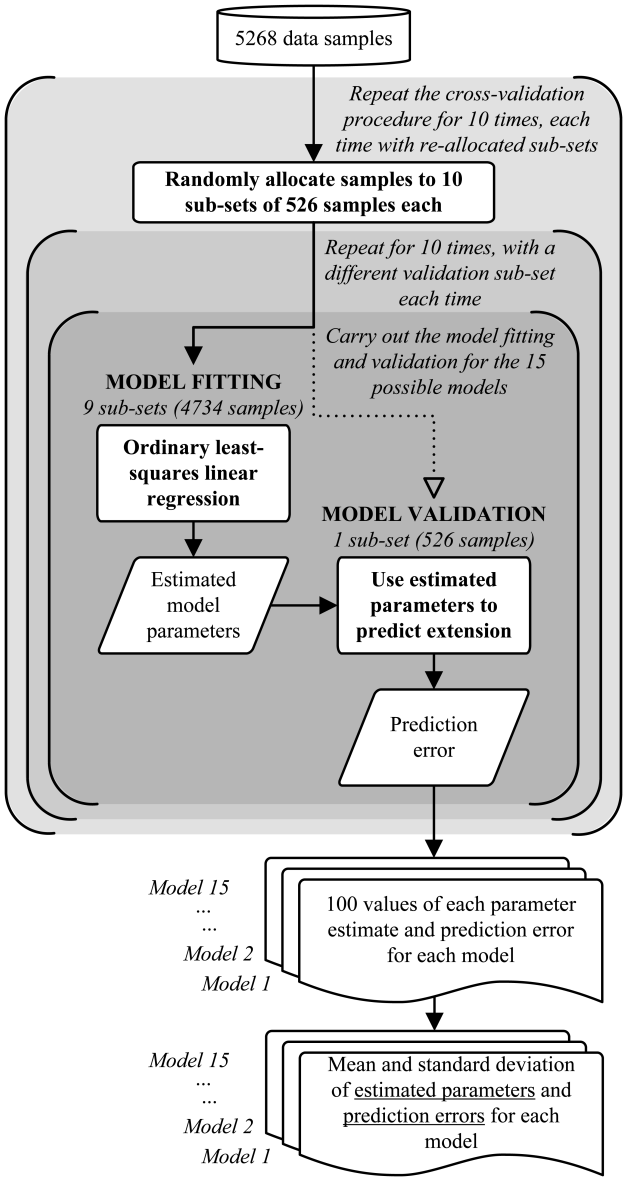

Figure 10. Schematic flowchart of the ten-fold cross-validation technique used to fit the temperature – extension linear polynomial models.

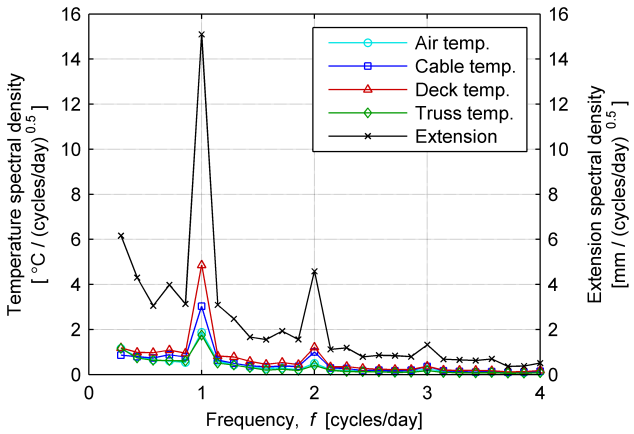

Figure 11. Auto amplitude spectral densities of the temperature and extension data, showing a predominant frequency of one cycle / day.

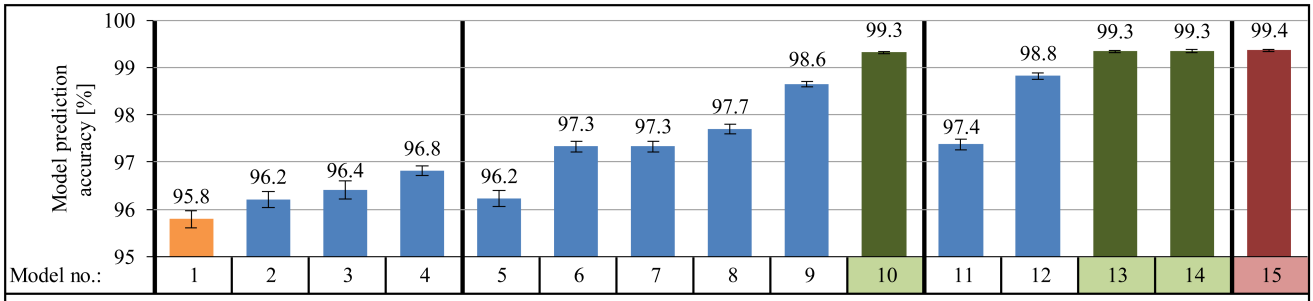

Model no.:	1	2	3	4	5	6	7	8	9	10	11	12	13	14	15
Number of temperature (T) variables used in the model	1				2						3				4
Estimated parameters for the model: $\hat{E}(t) = \hat{\beta} + \{\hat{\alpha}_{air} T_{air}(t) + \hat{\alpha}_{cable} T_{cable}(t) + \hat{\alpha}_{deck} T_{deck}(t) + \hat{\alpha}_{truss} T_{truss}(t)\}$															
$\hat{\alpha}_{air}$ [mm/°C]	-5.90	-	-	-	-0.97	-2.56	-	-	-2.55	-	-1.31	-2.13	0.51	-	0.41
$\hat{\alpha}_{cable}$ [mm/°C]	-	-	-5.29	-	-	-3.07	-2.82	-2.38	-	-	-2.85	-0.89	-	-0.30	-0.26
$\hat{\alpha}_{deck}$ [mm/°C]	-	-	-	-4.68	-	-	-	-2.63	-2.76	-2.60	-	-2.31	-2.62	-2.47	-2.50
$\hat{\alpha}_{truss}$ [mm/°C]	-	-5.95	-	-	-4.98	-	-2.85	-	-	-2.77	-1.52	-	-3.26	-2.61	-3.02
$\hat{\beta}$ [mm]	91.40	94.80	92.86	85.60	94.32	93.04	94.47	89.40	89.13	90.93	93.81	89.98	91.15	91.10	91.25
Prediction errors E - $\hat{E}$															
Max. [mm]	32.9	30.8	33.4	19.1	30.8	20.8	19.9	17.7	10.4	4.7	20.0	9.9	4.3	4.8	4.4
RMSE [mm]	7.1	6.4	6.1	5.4	6.4	4.5	4.5	3.9	2.3	1.2	4.5	2.0	1.1	1.1	1.1
Standard deviation of the prediction accuracy, as shown by the error bars															
[%]	0.18	0.17	0.19	0.10	0.17	0.12	0.11	0.11	0.06	0.03	0.11	0.06	0.02	0.03	0.02

Figure 12. The model parameters, prediction accuracy and prediction errors of the 15 temperature – extension linear polynomial models derived from the cross-validation analysis.

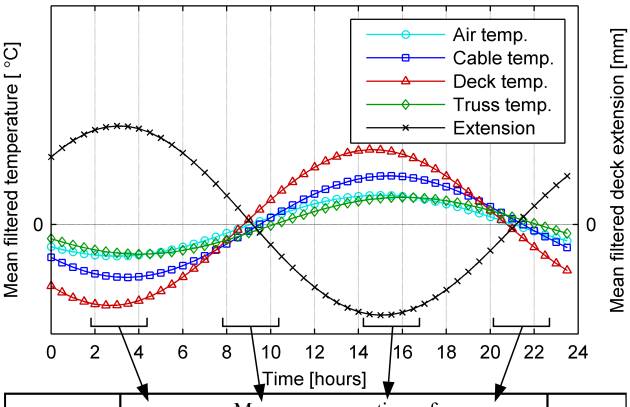

	Mean occurance time of				Mean delay
	1st peak	1st 0-cross.	2nd peak	2nd 0-cross.	
Air temp.	03 : 00	09 : 05	15 : 00	21 : 04	ref.
Cable temp.	03 : 30	09 : 29	15 : 30	21 : 29	27 min
Deck temp.	02 : 30	08 : 46	14 : 30	20 : 45	-25 min
Truss temp.	04 : 00	10 : 09	16 : 00	22 : 09	62 min
Extension	03 : 00	09 : 10	15 : 00	21 : 10	3 min

Figure 13. The smoothed daily temperature and extension cycles after bandpass filtering and averaging (top plot); and the peak times, zero-crossing times and resulting mean delays of each variable with respect to the air temperature (bottom table).

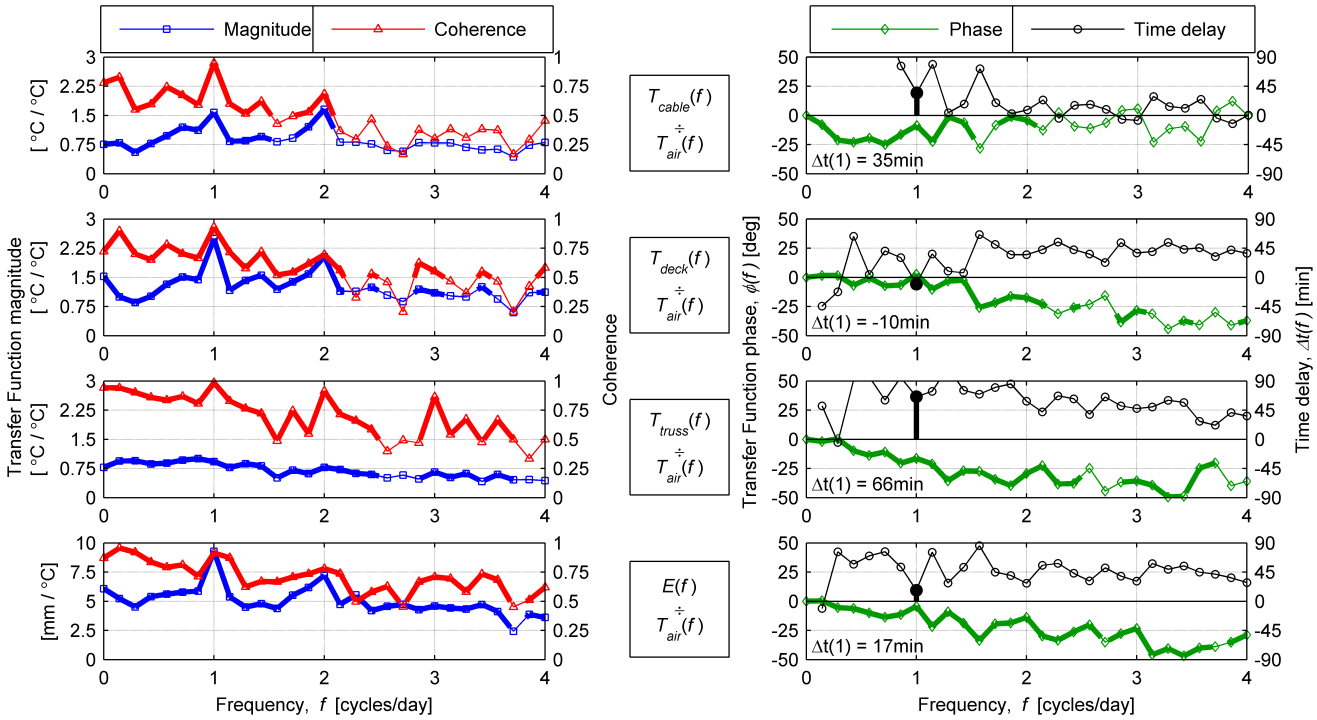

Figure 14. The coherence, magnitude and phase of the transfer functions and the estimated time delay between the air temperature (input) and the structural temperatures and deck extension (outputs). Thick lines indicate that the input and output variables are correlated (coherence ≥ 0.5).

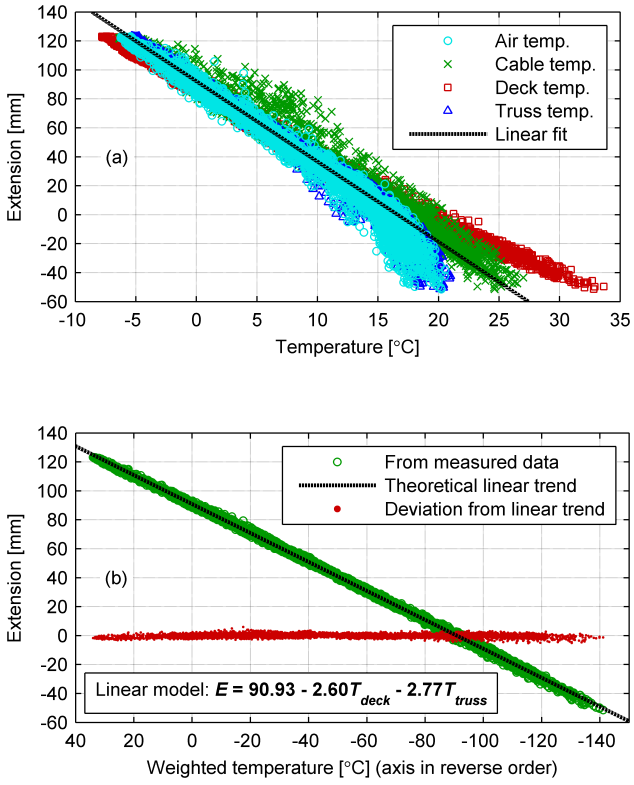

Figure 15. The deck extension plotted against (a) the individual temperatures; and (b) the combined deck and truss temperatures weighted according to the linear model in equation (8); showing the improvement in accuracy achieved by using the derived empirical model.

	Maximum		Minimum		Peak to peak	
	Value	Date	Value	Date	Value	Date
Air temp. [°C]	21.3	16 Aug	-6.6	07 Dec	12.3	21 Oct
Cable temp. [°C]	27.1	03 Sep	-6.6	07 Dec	18.3	30 Aug
Deck temp. [°C]	34.0	23 Jul	-8.1	07 Dec	26.9	30 Aug
Truss temp. [°C]	21.4	16 Aug	-5.6	07 Dec	11.7	21 Oct
Deck ext. [mm]	123.5	26 Dec	-52.4	25 Jul	83.3	23 Jul

Table 1. Maximum, minimum and largest daily peak to peak values of temperatures and deck extension recorded between July and December 2010 (maximum extension corresponds to largest deck contraction, minimum extension corresponds to largest deck expansion).

EC1 / UK National Annex (NA) clause	Calculation	Result
6.1.1(1)	Bridge is type 1 (steel deck on steel truss structure).	
6.1.3.2 & NA.2.5	Shade air temperatures for Plymouth (from isotherms): $T_{\min} = -10°C$; $T_{\max} = 31°C$	
NA.2.4 6.1.3.1(4) 6.1.3.1(4)	Uniform bridge temperature component: • Adjustment to $T_{\min}$ and $T_{\max}$ for deck surfacing < 100 mm = 0°C • Reduction to $T_{\max}$ for steel truss deck = 3°C $T_{e,\min} = -13°C$; $T_{e,\max} = 47 - 3 = 44°C$	
6.1.3.3(3) 6.1.3.3(3)	Range of uniform bridge temperature component: • Adjustment to $T_{e,\min}$ and $T_{e,\max}$ for bearings and expansion joints = 20°C $\Delta T_N = T_{e,\max} - T_{e,\min} + 40 = (44 + 20) + (13 + 20) = 97°C$	
	Design value of deck expansion: • Unrestrained length, $L = 449m$ • Coefficient of linear thermal expansion, $\alpha_L = 12 \times 10^{-6} m/m/°C$ $\Delta L = \alpha_L \cdot L \cdot \Delta T_N = 12 \times 10^{-6} \cdot 449 \cdot 97 = 0.5226m = 522.6mm$	$\Delta L = 522.6mm$

Table 2. Calculation of the design value for longitudinal deck thermal displacement following the recommendations in Eurocode 1 (European Committee for Standardization, 2003) and the UK National Annex (British Standards Institution, 2007).

	Air temperature measured / used			Deck extension measured / predicted		
	Maximum [°C]	Minimum [°C]	Range [°C]	Maximum [mm]	Minimum [mm]	Range [mm]
i) Measured	21.3	-6.6	27.9	123.5	-52.4	175.9
ii) Model prediction	21.3	-6.6	27.9	125.6	-51.3	176.9
iii) EC1 prediction	54.3	-29.6	83.9	NA	NA	452.1
iv) EC1 design value	64.0	-33.0	97.0	NA	NA	522.6
v) AASHTO design value	48.9	-34.4	83.3	NA	NA	437.8

Table 3. Temperature and deck extension extremes and overall range: (i) from acquired data; (ii) as predicted using the linear model in equation (8) from the acquired temperature data; (iii) as predicted using the Eurocode 1 (EC1) procedure based on the acquired temperature extremes; (iv) the design value calculated using the EC1 procedure based on local isotherm records; and (v) the design value calculated using the AASHTO procedure based on the recommended temperature range for cold climates. The temperatures used to obtain the EC1 values (iii) and (iv) include the safety factors specified in the code.